



“Gheorghe Asachi” Technical University of Iasi, Romania



APPLICATION OF ELECTRICAL RESISTIVITY IMAGING (ERI) TO INVESTIGATE AN OIL CONTAMINATED EXPERIMENTAL SITE

Bokani Nthaba, Elisha Shemang*, Oathusa Gareutlwane, Loago Molwalefhe

Earth and Environmental Science Department, Botswana International University of Science
and Technology, Palapye, P/Bag 16, Palapye, Botswana

Abstract

In this study we present time-related 3D ERI models for a site that was contaminated using waste automobile engine oil. The pristine geo-electrical characteristics of the site were recorded before the contamination was carried out. The purpose of the study was to progressively monitor the geo-electrical responses of the site for possible natural bio-transformations on the waste oil. Data were acquired once every two weeks for a period of three months using eight parallel 2D resistivity profiles. The 2D profiles were later inverted to 3D resistivity models of the contaminated site. The 3D inverse resistivity models indicated highest electrical resistivity values in zones that were heavily contaminated with the waste oil. We report progressive reduction in the resistivity of the subsurface in subsequent models after the fourth week of monitoring. The changes were potentially resulting from transformation of the waste engine oil due to enhanced microbial activity which in turn depends on optimal pH, sufficient nutrients and soil temperature. We also observed depleted nitrate concentrations and lower EC values compared to initial soil conditions, which is a sign that microbes are active and biodegradation is likely to be occurring. This study demonstrates the utility of the ERI method in monitoring hydrocarbon contaminated sites for potential degradation due to bio-remediation. Further research is however needed to illustrate the link between microbial degradation of the waste oil and the observed electrical resistivity changes, and related biogeochemical processes.

Key words: biodegradation, contamination, electrical resistivity imaging, isosurface, time-lapse

Received: November, 2018; *Revised final:* May, 2019; *Accepted:* May, 2019; *Published in final edited form:* December, 2019

1. Introduction

Numerous industrial activities require the use of hydrocarbon products to enhance economic output and uplift human welfare. Many such products accidentally end up contaminating the subsurface in many areas of work worldwide through spills, leaks and uncontrolled disposals (Ch and Chandrashekar, 2014; Tait et al., 2004; Von Lau et al., 2018). The spills move through the unsaturated zones of the subsurface as discrete accumulations due to their non-uniform dispersion through soils of variable permeability and the chemical properties (Ch and Chandrashekar, 2014; Domenico and Schwartz, 1998). Factors such as media capillarity (porous

and/or fractured), rainfall, hydraulic gradient and groundwater level of the contaminated areas have great influence on the migration potential of hydrocarbon products in the subsurface (Daniels et al., 1995). Beneath the water table, hydrocarbon products migrate through permeable pathways such as unconsolidated soil and rock fractures, and root holes that tend to provide slight capillary resistance to flow (Asiabadi et al., 2018; Gebrekristos et al., 2008).

Traditionally, assessment of oil polluted sites involved discrete point sampling using wells and piezometers along the anticipated migration paths. However, sparse piezometers and monitoring wells make it difficult to effectively determine the spatial distribution of oil or similar contaminants. Also,

* Author to whom all correspondence should be addressed: e-mail: shemange@biust.ac.bw; Phone: +267 4931542; Fax: (+267) 4900102

managing the resulting subsurface and/or groundwater contamination is difficult, in part due to the problems associated with acquiring the accurately representative datasets to decipher contaminant behavior within the system. The dual presence of fractured bedrock and heterogeneous strata compounds the difficulty in characterizing the contaminated sites using these conventional site investigation methods.

In order to assess and manage the risk that contamination may pose at industrial and/or agricultural sites, it is necessary to develop a good understanding of the nature and distribution of spills and contaminants in the subsurface. Early detection on the contaminants and their behaviors in the subsurface may be achieved by acquiring information with ameliorated spatial and temporal resolution. It is particularly paramount to appraise the contaminant-influenced subsurface changes and contaminant degradation due to microbial activity in an environment with semi-arid climate, as most documented research works which reported significant biodegradation of hydrocarbon contaminants have been conducted in cryophilic environments in temperate regions (e.g. Abdel Aal et al., 2004; Allen et al., 2007; Atekwana et al., 2000; Atekwana et al., 2002; Atekwana et al., 2004a, 2004c, 2004d; Atekwana and Atekwana, 2010, and references therein; Benson et al., 1997; Caterina et al., 2017; Delille et al., 2004; DeRyck et al., 1993; Pelletier et al., 2004; Yang et al., 2007) while very few studies have been documented on arid or semi-arid regions. This study adds to the few studies conducted on semi-arid environments.

Atekwana and Atekwana (2010) in particular, alluded to that the geophysical properties of hydrocarbon contaminated sites over time periods of months or even years after spills have occurred are related to the extent of physical, chemical and biological alteration of the contaminant. The authors further suggested that the degree of contaminant alteration will depend on the environmental conditions as determined by subsurface geology and climate. Therefore, there is a need for the use of non-invasive geophysical techniques to investigate hydrocarbon contaminated sites in semi-arid environments (as is the case in the present study).

Geophysical techniques estimate subsurface physical properties (density, resistivity, magnetic susceptibility, etc.) and may be useful in investigating environmental problems such as oil spills and related uncontrolled hydrocarbon products disposals in the subsurface. Among the geophysical methods, electrical resistivity imaging (ERI) technique has proved to be the most effective in delineating contaminated areas (e.g. Abdel Aal et al., 2004; Allen et al., 2007; Atekwana et al., 2000; Atekwana et al., 2002; Atekwana et al., 2004a, 2004c, 2004d; Atekwana and Atekwana, 2010; Benson et al., 1997; Caterina et al., 2017; Yang et al., 2007). ERI technique is a non-invasive technique which is used to estimate and present 2D/3D models of the subsurface electrical resistivity distribution. The resistivity of the

subsurface strongly depends on porosity, degree of saturation and pore fluid conductivity (Seferou et al., 2012). In this method, current is injected into the ground via a pair of current electrodes and the resulting potential difference is measured between another pair of potential electrodes. The observed data can then be used to locate zones contaminated by hydrocarbon products such as waste engine oil and also help monitor their migration with time in time-lapse measurements context.

The collected datasets are inverted to reconstruct the 2D/3D resistivity distribution of the subsurface using non-linear inversion methods (Loke and Barker, 1996). Relatively new (few months to a year) oil spillages usually manifest as resistivity highs in the electrical resistivity measurements whereas old and mature spills manifest as resistivity lows (Ch and Chandrashekar, 2014), hence their ability for detection and differentiation with the ERI method. The regular acquisition of 3D ERI measurements (time-lapse 3D ERI) can provide a measure of the temporal changes of the subsurface resistivity, and can aid the monitoring of oils or hydrocarbon migration in the subsurface with time (Ch and Chandrashekar, 2014).

Time-lapse electrical resistivity measurements have been used successfully in several environmental studies (e.g., Dahlin and Johansson, 1995; Johansson and Dahlin, 1996; Panthulu et al., 2001; Song et al., 2005). An advantage of time-lapse electrical resistivity measurements is the improved discrimination derived from interpretation of the electrical resistivity structure with respect to the initial structure. This comparative approach focuses on the differences between the datasets using changes in the electrical resistivity model and suppresses artifacts in the electrical resistivity structure (Loke, 1999).

To study the subsurface resistivity changes with time, repeated two dimensional (2D) electrical resistivity measurements are typically acquired over the same profiles (Karaoulis et al., 2011; Loke, 1999; Tsourlos et al., 2003).

The main objective of the present study is to investigate the applicability of 3D ERI in detecting engine oil spills and tracking the plume movement in the experimental area. Time-lapse 3D ERI method using parallel 2D profiles was employed for better spatial and depth resolution of the resulting images.

The utility of combining geoelectrical responses of the subsurface with geochemical measurements at areas affected by hydrocarbon contamination cannot be over-emphasized (e.g. Atekwana et al, 2014; Noel et al., 2016; Schwartz et al., 2014).

Interpretation of geophysical data for biophysicochemical processes can be challenging because several factors of the subsurface environment (metals, presence of clays, soil pore water saturation, etc.) contribute to the electrical response. Geochemical measurements have therefore become a validating tool in many such studies to assess indirectly zones of enhanced biodegradation.

2. Material and methods

2.1. Experimental setup

An ideal experimental site for demonstrating the utility of ERI to monitor hydrocarbon contamination would have both homogeneous electrical resistivity and hydrogeological properties. In that case, ERI would show a uniform distribution of electrical resistivity in the background/baseline data images acquired before the pit excavation and the oil spill, and the local hydraulic gradient would uniformly drive groundwater flow (Comfort et al., 2009). Additionally, the contaminant should be distributed such that it can be clearly identifiable in the test site, and should cause a large enough change in the electrical resistivity to be detected by the ERI technique (Comfort et al., 2009). The experimental site (22.5946° S, 27.1233° E) for the current study (Fig. 1a) fulfilled the criteria listed above. Based on lab analysis of collected soil samples from the pit excavation, the site was described to be dominated by

clayey loam soil displaying minimal grain size variation to a maximum excavated depth.

A pit with dimensions 2 m by 4 m by 2 m was excavated (Fig. 1b) in order to loosen the soils and prepare an impervious base. The pit was sealed at the base and the lower walls with a plastic membrane to stop the engine oil from descending beyond the 2 m depth. The pit was then refilled with the same excavated material to about 0.3 m below the ground level and waste oil of about 30 Litres was then spilled randomly in the pit (Fig. 1c) before entirely burying it (Fig. 1d). Parallel 2D ERI lines were then established to acquire electrical resistivity measurements (Fig. 1e).

Usually, these contaminants are disposed directly in the soil posing a high risk to the environment. Impermeability of the pit base and the lower walls is mandatory for preventing leaking of engine oil to the subsurface with the potential to pollute groundwater. Industrial and/or agricultural sites should have impermeable rocks and non-tectonic regime (Seferou et al., 2012) to avoid contamination of the subsurface (unsaturated zone) and the aquifer.



Fig. 1. (a) satellite image of the broader study area and the experimental site, (b) excavation of the pit of dimensions 2 m width by 4 m length and 2 m depth, (c) the refill of the pit with the same excavated material and engine oil spillage surface at a depth of 0.3 m from ground surface, (d) burial of the engine oil with the original excavated material of the area up to the ground level and (e) photograph of a 2D resistivity data acquisition setup. Also shown is an insertion of the layout of 8 parallel 2D profiles

However, in most cases these industrial sites are usually composed of unconsolidated material such as sandy soils, gravels and pebbles. In this study, the experimental site is located on clays and clay dominated soils, which tend to delay percolation of pollutants in the subsurface. The dissolution of a contaminant into the groundwater significantly affects groundwater quality (Seferou et al., 2012). Dissolution is one of the fundamental mass transfer processes that occur when oil is spilled on water (Bobra, 1992). Therefore, we decided to loosen the soils and irrigate the site with water on regular basis in order to simulate a real case study while we continuously acquire time-lapse measurements.

2.2. D ERI data acquisition

Firstly, we established eight (8) permanent resistivity profiles on the experimental site and used an array of 48 stainless steel electrodes that were planted 10 cm into the ground. The initial resistivity dataset was acquired before the pit was excavated using an Iris Syscal Pro resistivity unit (on the 11th February, 2017). The electrode spacing was 0.17 m while line spacing was 0.5 m (Fig. 1e). The electrode spacing used generated 7.99 m long profiles that imaged to a depth of approximately 1.73 m. Four subsequent electrical resistivity measurements were acquired on a two-week interval basis: 18th February, 2017; 4th March, 2017; 18th March, 2017 and; 1st April, 2017, after the pit was dug and polluted with engine oil.

Because of its better resolution to lateral changes along the profiles, the dipole-dipole array was used in this experiment to resolve the downward movement of the engine oil (downward electrical resistivity changes). The maximum depth of investigation we were interested in was 1.73 m. Electrode positions on the site were maintained whenever measurements were taken to minimize errors associated with misplacement of electrodes over time. Tests before acquisition were performed for each profile and the results indicated that the site provided good coupling with contact resistances generally below 3 k Ω . A transmitter-current injection time window (T_n) of 4 seconds was chosen and 3 to 6 stacks performed with a quality factor (i.e., the standard deviation of the stacked signal) of 3 %. It was anticipated that the engine oil would cause large resistivity anomalies in the subsurface, and it was assumed that the oil movement would be enhanced in nonconsolidated subsurface soils.

2.3. D ERI data processing

The 2D electrical resistivity data collected along the eight profiles, each with 906 data points were combined into a single text file. The text file created was used in Res2Dinv software to collate data into Res3Dinv formatted data file that was then inverted to reconstruct the 3D model. This procedure

was repeated for the base line measurements and after the oil spillage into the test site. To obtain good inversion models, we removed bad data points from the data set using a statistical technique, through the RMS error statistics option. It is expected bad data points will have relatively large errors, e.g. above 100 % (Loke, 2009).

In this study, only data points with apparent resistivity percentage errors of 21 % or less were used and yielded final inversion resistivity models with RMS errors ranging from 4.2 % to 9.4 %. The five 3D datasets were inverted independently using the robust inversion with the standard least-squares model constraint, which attempts to minimize the square of the difference between the measured and calculated apparent resistivity values (Loke, 2009). We expected electrical resistivity properties of the subsurface to change in a smooth manner even after oil contamination due to the minimal variation observed within the soil profile, hence the choice of this model constraint.

We used two 3D inversion software packages: 3D Electrical Resistivity Tomography (ERTLabTM) inversion software developed by Multi-Phase Technologies and Geostudi Astier, to display high resistivity anomaly isosurface models, and the Res3Dinv $\times 64$ basic version by GeotomoTM software to invert and generate the horizontal (x-y) plane resistivity distribution sections of the subsurface. The Res3Dinv inversion software can only plot the inversion model in the form of horizontal or vertical slices through the earth, and model values stored in the inversion file are usually exported to a variety of 3D display and contouring software, hence the use of ERTLabTM software in this study.

2.4. Soil chemo-physical properties

The soil pH and the electrical conductivity were determined after the samples were added to deionized water and left to sonicate for 6 hours. At the end of 6 hours the mixture was sampled for measurements pH and the electrical conductivity (EC). Samples were filtered through a 45 μm nylon filter and measurements determined using the Hanna HI 9811-5 pH/EC meter. Nitrate levels were determined after digesting the soil samples using ammonium acetate for 3 hours. Samples were then filtered before measurements were undertaken using the ICS Dionex 5000 ion chromatograph. The EC represents the sample bulk chemistry changes while the choice of nitrate was based on the fact that oil spills cause dramatic decrease in the nutrients levels as nutrients are essential for bacterial metabolism (Dibble and Bartha, 1979) during transformation of hydrocarbons to minerals (Thavasi et al., 2007). Soil samples that were not contaminated with oil were collected as experimental controls to ensure that the natural environment at the site did not undergo similar processes that would significantly influence the results of the experiment.

3. Results and discussion

3.1. Resistivity models

The electrical resistivity investigation of the experimental site generated horizontal (x-y plane) resistivity distribution sections of the subsurface. 3D resistivity models derived from Res3Dinv software are shown in Fig. 2 to Fig. 7.

Figs. 2-3 display the horizontal slices of the initial dataset (before the excavation/background). The third dimension (depth) is given in numerical form above the respective horizontal slices. The 2D horizontal slices show lateral and vertical electrical resistivity variation within the experimental site. Two prominent anomalous zones are observed in all the displayed horizontal slices. The first anomalous zone is characterized by resistivity values ranging from 3.5 Ω m to 29.1 Ω m, while the second anomalous zone

shows resistivity values ranging from 29.1 Ω m to 58.9 Ω m. These were interpreted to represent the background material (clay-dominated soils) with either varying moisture content or cohesion between soil particles.

In Fig. 2, isolated spots of high resistivity values (119-489 Ω m) are evident, but only limited to layer 1 (Fig. 2a) and layer 2 (Fig. 2b). Layer 1 and layer 2 are composed largely of an assortment lower resistivity anomalies (3.5-58.9 Ω m), interpreted to be representing clay dominated soils with a limited number of small, isolated high resistivity zones (119-489 Ω m), probably due to variations in moisture content. From layer 3 (Fig. 2c) to layer 6 (Fig. 2f), and from layer 7 (Fig. 2a) to layer 12 (Fig. 2f), the area is composed entirely of two distinct low electrical resistivity anomalies (3.5-29.1 Ω m and 29.1-58.9 Ω m), in varying patterns, also representing clay or clay-dominated subsurface soils.

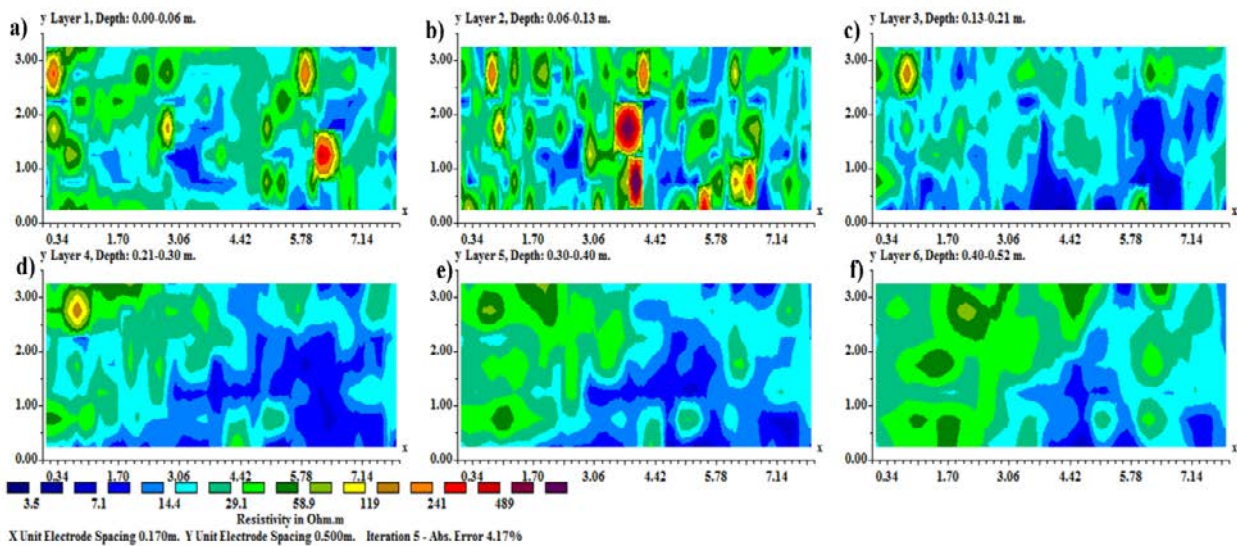


Fig. 2. The inversion model for the initial dataset (acquired on the 11th of February, 2017) displayed as x-y plane horizontal slices for (a) layer 1 (depth: 0.00- 0.06 m), (b) layer 2 (depth: 0.06- 0.13 m), (c) layer 3 (depth: 0.13- 0.21 m), (d) layer 4 (depth: 0.21- 0.30 m), (e) layer 4 (depth: 0.30- 0.40 m) and (f) layer 6 (depth: 0.40- 0.52 m)

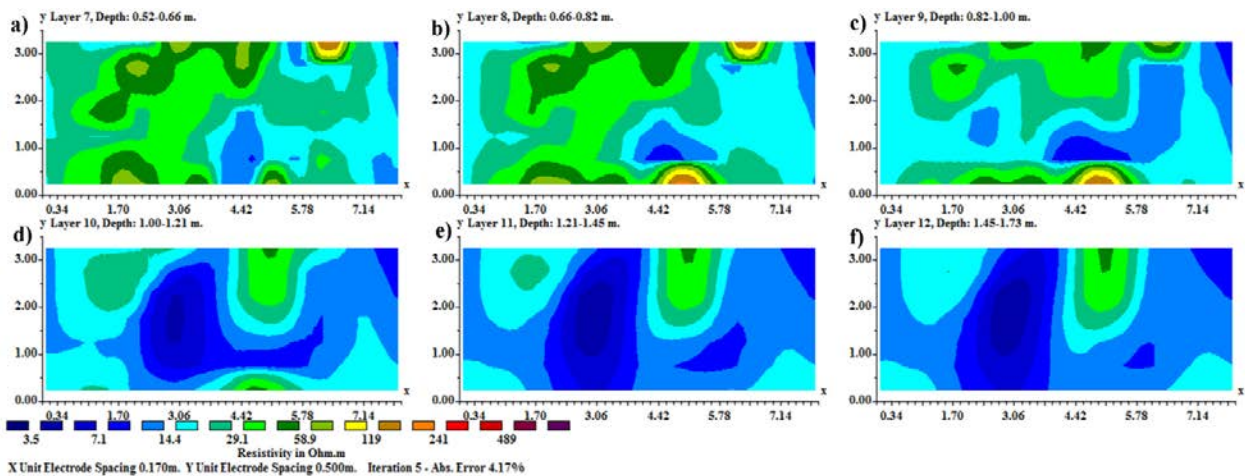


Fig. 3. The inversion model for the initial dataset (acquired on the 11th of February, 2017) displayed as x-y plane horizontal slices for (a) layer 7 (depth: 0.52- 0.66 m), (b) layer 8 (depth: 0.66- 0.82 m), (c) layer 9 (depth: 0.82- 1.00 m), (d) layer 10 (depth: 1.00- 1.21 m), (e) layer 11 (depth: 1.21- 1.45 m) and (f) layer 12 (depth: 1.45- 1.73 m)

Fig. 4 depicts the lateral and vertical electrical resistivity variation within the experimental site (background and contaminated zones) for the second dataset, acquired on the 18th of February, 2017. Layer 1 (Fig. 4a) clearly shows a regularly shaped low resistivity zone (3.5-7.1 Ωm) correlating well with the refilled pit at the test site. Flanking the pit is a zone of intermediate resistivity values ranging from 29.1 Ωm to 58.9 Ωm representing the background area of the experimental site. Also observed on the perimeter of the low resistivity zone are isolated spots of high resistivity values of about 119 Ωm to 489 Ωm , likely to represent small-scale oil contaminated zones.

Layer 2 (Fig. 4b) comprises of an assortment of low-high resistivity values. On layer 3 (Fig. 4c) there are lenses of high resistivity values (119-489 Ωm) within the pit region indicating the zone contaminated with engine oil (just above the 0.3 m engine oil burial depth), and this high resistivity anomaly is prominent within layer 4 (Fig. 4d) and layer 5 (Fig. 4e), corresponding with the engine oil spillage surface within the pit.

We observe a diminishing high resistivity zone in layer 6 (Fig. 4f), and from layer 7 (Fig. 5a) to layer 9 (Fig. 5c), and completely fades from layers 10 (Fig. 5d) to layer 12 (Fig. 5f), suggesting very minimal to non-existent oil contamination in the lower zones of the experimental site. Figs. 6-7 show x-y plane horizontal slices obtained from the Res3Dinv inversion software. Electrical resistivity distribution follows a similar pattern in the first two layers (layer 1 and layer 2). However, layer 1 (Fig. 6a) shows a more pronounced low resistivity zone (3.5-7.1 Ωm), corresponding to the pit area, while the same anomaly diminishes in layer 2 (Fig. 6b), with relatively small-scale low-intermediate (29.1-58.9 Ωm) resistivity zones emerging on the edges of the low resistivity zone, attributable to zones slightly contaminated by engine oil.

The high resistivity anomaly (119-489 Ωm) prominent in the central part of layer 3 (Fig. 6c) and

layer 4 (Fig. 6d) indicates a zone significantly contaminated by oil. Conversely, the size of the high resistivity zone is steadily reducing from layer 5 (Fig. 6e) to layer 6 (Fig. 6f), and completely fades in lower/relatively deeper layers (Fig. 7a to Fig. 7f), suggesting an insignificant to non-existent oil contamination in the lower zones of the experimental site.

3.2. Resistivity isosurfaces

The final ERT 3D resistivity inversion models, generated using the ERTLabTM inversion and modeling software are presented using the isosurface presentation (Fig. 8). Five different time steps are presented to show the zones affected by the contaminant (engine oil) in the subsequent datasets, and the contaminant movement over time.

Fig. 8a shows the initial dataset model and does not show contamination as it represents only background resistivity measurements outside the plotted high resistivity anomaly isosurface range of 119 Ωm to 489 Ωm , while in Figs. 8b, 8c, 8d, and 8e, we observe emergence of a zone of relatively higher resistivities ranging from approximately 119 Ωm to about 489 Ωm , indicating an anomaly of interest (contaminated zone) in the 3D resistivity model. This high resistivity anomaly was then made to stand out in a full 3D model (isosurface) while suppressing the lower resistivity values.

3.3. Soil chemo-physical characteristics

The chemo-physical characteristics of the soil from different depth are shown in Table 1. The measured changes were in the pH, EC, and nitrate concentration for the contaminated site as well as for the standard. In general, the EC showed increments between samples that were collected at the beginning and end of the experiment over the two-year period. Only the surface soil sample (0-10 cm) showed some decrease over the same period.

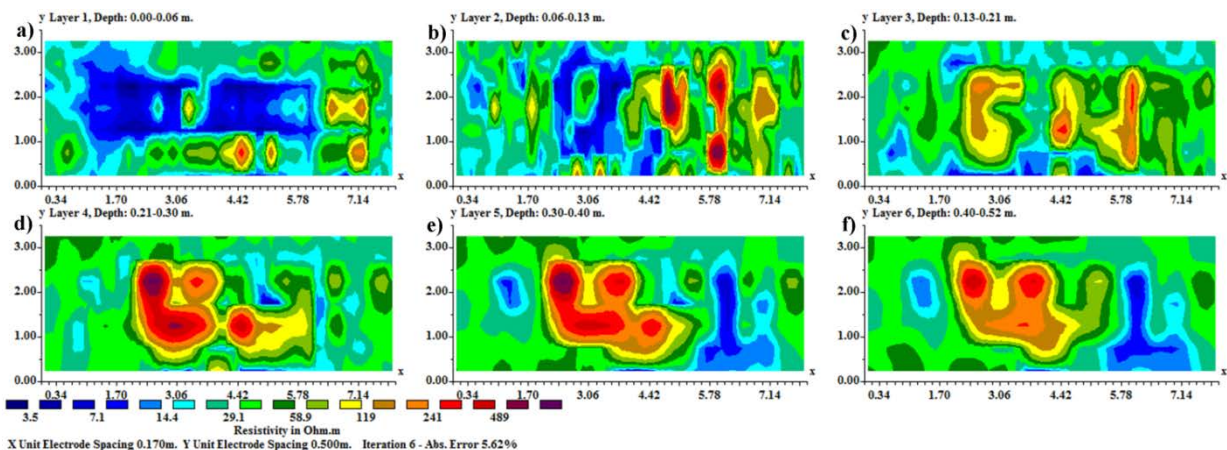


Fig. 4. The inversion model for the second dataset (acquired on the 18th of February, 2017) displayed as x-y plane horizontal slices for (a) layer 1 (depth: 0.00- 0.06 m), (b) layer 2 (depth: 0.06- 0.13 m), (c) layer 3 (depth: 0.13- 0.21 m), (d) layer 4 (depth: 0.21- 0.30 m), (e) layer 4 (depth: 0.30- 0.40 m) and (f) layer 6 (depth: 0.40- 0.52 m)

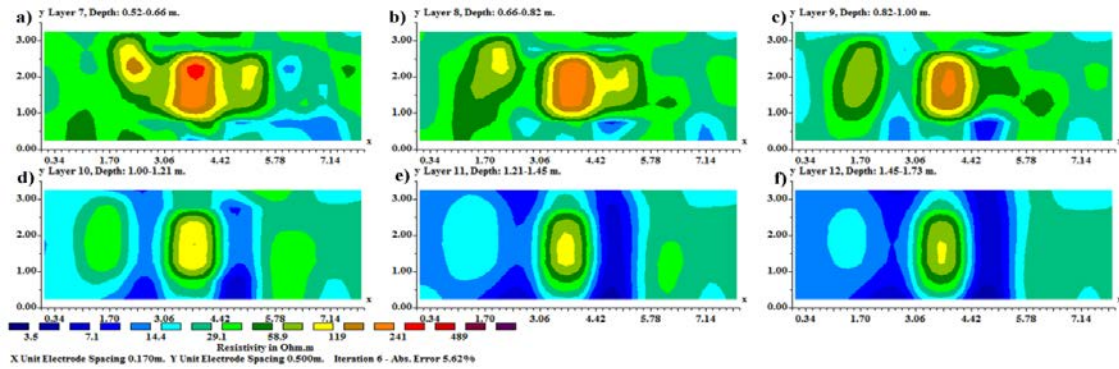


Fig. 5. The inversion model for the second dataset (acquired on the 18th of February, 2017) displayed as x-y plane horizontal slices for (a) layer 7 (depth: 0.52- 0.66 m), (b) layer 8 (depth: 0.66- 0.82 m), (c) layer 9 (depth: 0.82- 1.00 m), (d) layer 10 (depth: 1.00- 1.21 m), (e) layer 11 (depth: 1.21- 1.45 m) and (f) layer 12 (depth: 1.45- 1.73 m)

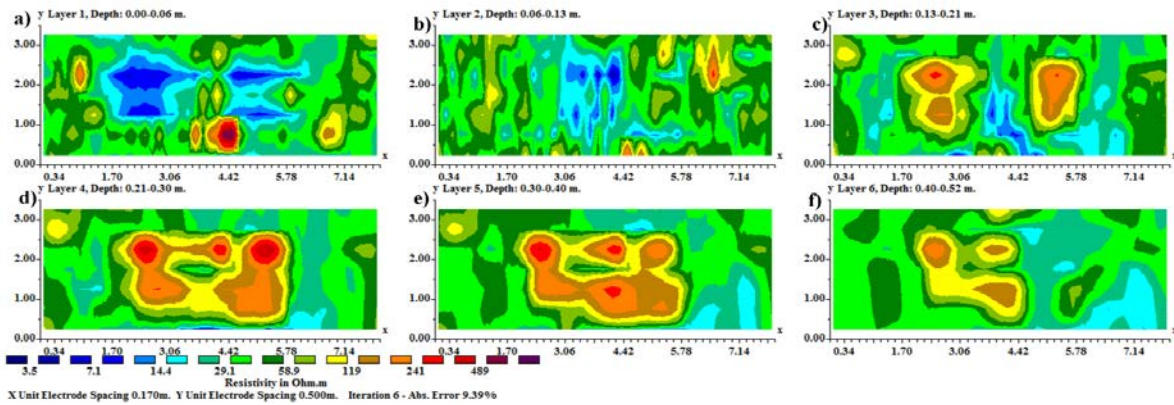


Fig. 6. The inversion model for the fifth dataset (acquired on the 1st of April, 2017) displayed as x-y plane horizontal slices for (a) layer 1 (depth: 0.00- 0.06 m), (b) layer 2 (depth: 0.06- 0.13 m), (c) layer 3 (depth: 0.13- 0.21 m), (d) layer 4 (depth: 0.21- 0.30 m), (e) layer 4 (depth: 0.30- 0.40 m) and (f) layer 6 (depth: 0.40- 0.52 m)

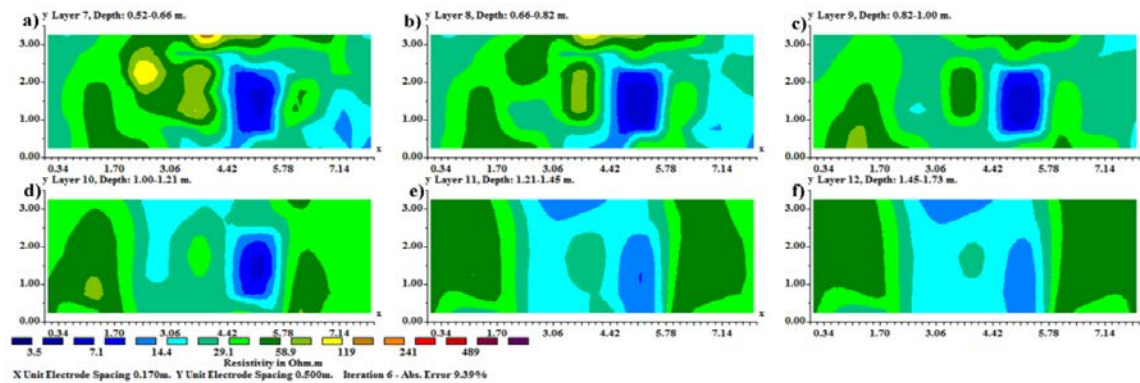


Fig. 7. The inversion model for the fifth dataset (acquired on the 1st of April, 2017) displayed as x-y plane horizontal slices for (a) layer 7 (depth: 0.52- 0.66 m), (b) layer 8 (depth: 0.66- 0.82 m), (c) layer 9 (depth: 0.82- 1.00 m), (d) layer 10 (depth: 1.00- 1.21 m), (e) layer 11 (depth: 1.21- 1.45 m) and (f) layer 12 (depth: 1.45- 1.73 m)

This zone was above the contaminated depth hence not affected by the oil degradation. Decreases in the EC at this zone may have resulted from leaching of soil minerals during site watering. All the depths below the contaminated zone showed increasing EC values after 22 months, indicating additions in the soil chemistry. The highest EC values occur at around 80 cm below surface and probably indicate an active zone of biological activity. The nitrate concentrations are higher for the depth 70-80 cm, and lower for shallower depths. Shallower depths have relatively lower EC values and are likely places where advanced

mineralization has taken place. The pH varied slightly between 7 and 8.

3.4. Analysis

The three dimensional (3D) survey through sets of equally spaced profiles along which electrical resistivity measurements were made enabled the generation of horizontal sections and isosurface models which show the distribution and variation of electrical resistivity along the two horizontal (x and y) and vertical (z) orthogonal directions.

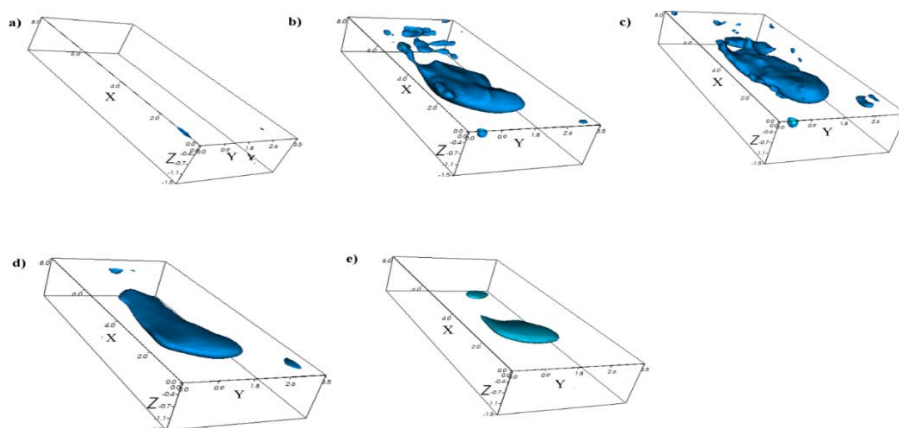


Fig. 8. Final 3D resistivity models from the ERTLab Viewer presented as isosurfaces for the datasets acquired on: (a) 11th of February, 2017, (b) 18th of February, 2017, (c) 4th of March, 2017, (d) 18th of March, 2017 and (e) 1st of April, 2017. Only relatively high resistivity (119-489 Ωm) isosurface is shown

Table 1. Snapshot of soil chemo-physical properties at various depths before and after contamination with waste automobile oil. The control site is located 7 meters from the experimental site and was sampled only at depth of 42-48 cm.

Sample Depth (cm)	2017			2019		
	pH (H ₂ O)	EC (μS/cm)	NO ₃	pH (H ₂ O)	EC (μS/cm)	NO ₃
0-10	7.6	530	52.87	7.1	510	0
42-48	7.7	540	171.66	7.5	730	115.29
61-67	7.7	530	78.70	7.3	860	28.20
70-80	7.9	650	113.51	7.5	1140	364.40
(Control) 42-48	7.7	240	18.63	7.5	320	18.72

Isosurface images in conjunction with electrical resistivity models/sections were made in order to properly fathom out the effect of engine oil as a contaminant in the subsurface. From the presented models (Fig. 2 to Fig. 7), it is apparent that subsurface investigated to a maximum depth of 1.73 m has slightly varying electrical resistivity distribution in the initial dataset models and resistivity varies significantly in the subsequent dataset models.

The isosurface images (Fig. 8) show the concentration of the contaminant in the middle of the 3D models, in an interval of 0.1 m to 0.8 m depth. As shown in these models, the zone affected by the engine oil was within the detection limit of the acquisition setup, and manifests as a high resistivity anomaly (119-489 Ωm), relatively higher than the maximum resistivity value (69.4 Ωm) recorded in the initial dataset acquired before oil contamination. These findings are consistent with previous investigations of hydrocarbon contaminated sites (Benson et al., 1997; DeRyck et al., 1993; Lien and Enfield, 1998; Mazác et al., 1990). In particular, the high resistivity anomaly associated with the engine oil contamination resembles the findings in a study conducted by Yang et al. (2007), where they investigated a field site with fresh LNAPL contamination which had resulted from an accidental underground pipeline leak in 1997. The authors observed much higher resistivity values of more than 140 Ωm in the contaminated region compared to less than 140 Ωm in the uncontaminated region. Light non-aqueous phase liquids are insulators (~10⁶ Ωm) relative to formation fluids (~10⁴-10³ Ωm)

(Atekwana and Atekwana, 2010), hence this findings. Also, the authors' observations may essentially be due to the fact that fresh hydrocarbon spills have not been significantly altered by biological or chemical processes. Atekwana et al. (2000) suggested that a considerable amount of time and sufficient alteration of hydrocarbon by environmental and biologic processes is required for the contaminated region to engender physical properties that sufficiently contrast with the background and a region contaminated by unaltered hydrocarbon contaminant.

In Fig. 8, no further high resistivity anomaly is observed beyond a depth of 0.8 m. However, the effect of the contaminant becomes unnoticeable at a depth of 0.8 m in the dataset models subsequent to the second dataset models. The contaminant effect is observed at depths of about: 0.6 m in the third dataset models; 0.45 m in the fourth dataset models and; 0.4 m in the fifth dataset models. We expected the high resistivity anomaly observed in a fresh engine oil contaminated site to continually grow with depth, no signs of biodegradation were expected in such a short period of monitoring. However, contrary to these expectations, the high resistivity anomaly observed in the second dataset model showed a decrease in size just one month after the oil spillage.

The decrease in size of the contamination plume observed in the third and subsequent dataset models may be attributable to a number of factors. Firstly, may be attributed to the saturation effects. Increased saturation from regular infiltration will decrease the resistivity of the sediments inundated

with water. Nonetheless, the electrical resistivity at the base of the contamination plume is expected to be higher in cases where ample hydrocarbon contaminant has occupied those bottom contaminated zones, since the partial replacement of water by oil will lower the water saturation, as a result increasing the electrical resistivity of those impacted zones (Abdel Aal et al., 2004; Lien and Enfield, 1998). We observe lower resistivities at the base of the contamination plume, opposite to the high resistivity observed in the second dataset model at the same zone. In fact, the size of the contamination plume had steadily decreased from the third dataset model to the final dataset model. Considering the duration of the experiment, these changes were not consistent with the expected growth of the high resistivity contamination plume to greater depth as the engine oil descends or partially replaces water in the saturated lower zones of the investigated area.

Secondly, the contamination plume shrinkage may also be attributed to microbial activity. Microbes are ever present in the subsurface and aboriginal microbes rapidly adapt to the use of a plethora of carbon from oil contamination or light non-aqueous liquids generally (LNAPL) (Atekwana and Atekwana, 2010). The effect of microbial activity on in-situ physical properties has been demonstrated in many studies conducted on hydrocarbon contaminated sites (Atekwana et al., 2000; Cozzarelli et al., 1990, 1994, 2001; Sauck et al., 1998; Shevlin et al., 2003; Werkema et al., 2003). Population numbers of oil degrading microorganisms tends to increase with depth zonation within contaminated soil columns (Atekwana et al., 2004). The observed decrease of high anomaly from the lower sections of the contaminated zone may be due to the enhanced mineral weathering attributable to the probable presence of specialized microbial community capable of degrading engine oil (Haack and Bekins, 2000). We therefore postulate that specialized microbial populations capable of degrading engine oil with increased efficiency are distributed at lower depths in the contaminated area.

The role of microbes in altering the physical properties of hydrocarbon contaminated sediments and the rate of bioremediation or microbial activity to be stimulated is not fully understood, hence there is need for more long-term time-lapse investigations of the contaminated areas, from the early days of hydrocarbon spills, either through controlled laboratory experiments or on natural field settings. In one study, in-situ microcosm experiments in a hydrocarbon contaminated aquifer showed that minerals were colonized by indigenous bacteria and chemically weathered at rates faster than theoretically predicted (Hiebert and Bennet, 1992). Additionally, an experiment conducted at a hydrocarbon contaminated area by Atekwana et al. (2004a) a five-fold increase in microbial numbers was reported in the diesel contaminated column in a narrow zone, within the second month after the experiment inception and observed an increase to a broader depth zone (30-65

cm) in later months. They suggested that the spatial (i.e., depth) increase was likely due to microbial succession (continuous change and adaptation of microbes to changing conditions) typically observed in organic contaminant plumes (Bekins et al., 1999). In the minimum resistivity zones, Atekwana et al. (2004a) document a higher percentage of oil degrading microbial populations. Also, Atekwana et al. (2004a) inferred from their results that the mechanisms for the low resistivity anomalies observed in hydrocarbon contaminated sediments is partly related to enhanced mineral weathering from metabolic by-products attributable to microbial degradation of the hydrocarbon.

A review of literature by Atekwana and Atekwana (2010) suggests that microbial processes greatly alter the contaminated environment causing marked changes in the petrophysical properties, mineralogy, solute concentration of pore fluids, etc. Numerous studies have corroborated the findings of anomalous geophysical signatures at hydrocarbon contaminated sites undergoing bioremediation (e.g. Allen et al., 2007; Atekwana et al., 2000, 2002; Atekwana et al., 2004a, 2004b, 2004c, 2004d).

Biodegradation of hydrocarbon contaminants is indeed a complex process that depends on the nature and on the amount of available hydrocarbons (Das and Chandran, 2011). The efficacy of biodegradation is determined by a number of factors, some of them having been reported in Cooney et al. (1985) and in Brusseau (1998). One important factor that influences biodegradation of oil pollutants in the environment is their availability to microorganisms (Das and Chandran, 2011). It is likely that the excess of organic carbon from engine oil contamination may have aroused activity of indigenous microorganisms, leading to significant alterations of the contaminated zone from the base upward. The activity of indigenous microorganisms naturally found in the hydrocarbon contaminated sites attenuates contaminants and transforms them into organic carbons and less toxic compounds (Atekwana et al., 2000; Atekwana et al., 2004; Chambers et al., 2010; Mazac et al., 1987; Urish, 1983). Temperature is suggested to be among the physical factors that have a significant impact in the biodegradation of hydrocarbons, as it does not only affect the chemical composition of pollutants, but also affects the physiology and diversity of microorganisms (Das and Chandran, 2011). Atlas (1975) reported that low temperatures reduced the viscosity of the toxic low molecular weight hydrocarbons, hence delaying the biodegradation initiation. Temperature also affects the solubility of hydrocarbons (Chaillan et al., 2004). Despite the wide range of temperatures at which hydrocarbon biodegradation occurs, lower temperatures generally decrease rates of biodegradation (Das and Chandran, 2011). Venosa and Zhu (2003) postulated that air temperature directly influenced the spilled oil properties and the microbial activity. This would explain the findings of this study, and why previous investigations of hydrocarbon contamination in

temperate regions show delayed evidence of microbial activity, only observable in aged contaminated sites.

Optimal pH and nutrients present at the contaminated sites are also valuable ingredients for the success and rate of biodegradation of hydrocarbon pollutants especially nitrogen, phosphorus and in some cases, iron (Cooney, 1984; Orozco, 2012). The observed pH varying slightly between 7 and 8 is an effective range for microbial activity and bioremediation of hydrocarbons (Thavasi et al., 2007). Microorganisms carry out the mineralization of organic chemicals by converting CO₂ and H₂O and biomass to salts. This process of mineral fixation changes the soil biophysical conditions which in turn modifies the ground electrical properties. Two zones of mineralization have been identified in this study. One is a zone of advanced mineralization characterized by lower nitrate levels and lower soil EC while the other is active with opposing soil chemical and electrical properties. In this case the soil electrical properties are expected to vary according to the level of mineralization whereby advanced mineralization is associated with lower electrical responses and lower nitrates levels.

Depleted nitrate concentrations and lower EC values compared to initial soil conditions are a sign that microbes are active and biodegradation is likely to be occurring (NRC, 1993). In this case, we observe that there has been more changes at the shallower depth, consistent with age (time). There is an agreement between the soil chemo-physical properties with the ERI profiles measured in the field. Within the zones of advanced mineralization we observe that the electrical resistivity of the soil is comparatively higher when compared to where there is active biological activity, i.e. less mineralization.

Further research is clearly needed to investigate the effect of microbial activity and more factors that influence its efficiency, microbial colonies or populations able to degrade oil and hydrocarbon biodegradation evidence on the engine oil contaminated site. Microbial populations are not a direct measure of biodegradation, but they provide a good measure of biodegradation potential of the hydrocarbon contaminated site sediments (Bossert et al., 1997).

4. Conclusions

3D ERI have been used successfully in this study to delineate fresh engine oil contaminated zones, determine the temporal variation of the electrical resistivity within the contaminated zone and to determine oil migration/degradation patterns in the subsurface. Though the ambiguous relationship between the modeled electrical resistivity and the light non-aqueous liquids is difficult to determine, there is an apparent relationship between the high electrical resistivity and the engine oil as a LNAPL for this experimental site.

Resistivity models generated in this study indicate that the waste engine oil contamination in the

subsurface was restricted to a depth range of 0.1 m to 0.8 m below the ground and reveal that zones that were heavily contaminated with waste engine oil had the highest electrical resistivity values (119 Ωm to 489 Ωm) in the initial datasets. However, in resistivity models of the datasets acquired after the fourth week of monitoring we observe electrical resistivity decrease in the contaminated zone occurring at discrete depth intervals, from the base of the contamination plume upwards. The observed resistivity decrease is likely resulting from transformation of the waste engine oil due to enhanced microbial activity which in turn depends on optimal pH, sufficient nutrients and temperature conditions, as it has been documented in numerous studies conducted in temperate regions (aged contaminants) and scarce reports in semi-arid regions. We also observed depleted nitrate concentrations and lower EC values compared to initial soil conditions, which is a sign that microbes are active and biodegradation is likely to be occurring.

This study showed that hydrocarbon contaminant is likely to be undergoing bioremediation, and there is a potential for time-lapse 3D ERI technique to be used in monitoring hydrocarbon contaminated sites in such situations. ERI is indeed a versatile geophysical method for delineating areas of biodegradation on sites where the subsurface is contaminated with hydrocarbons. Shallow areas with advanced biodegradation show higher mineralization and therefore have higher resistivity values. Areas of less mineralization are areas of active biological activity and manifest as lower electrical resistivity anomalies in ERI measurements. Considering our findings, further research combining biological, geochemical and hydrologic information is needed to have proper insights on biodegradation factors, microbial numbers, cultures and a variety of microorganisms able to degrade engine oil and present at the site.

Acknowledgements

Botswana International University of Science and Technology provided funding for this research. The authors acknowledge Mr. Boniface Kgosidintsi and Mr. Phenyio Tlale for their priceless efforts to make this project a success.

References

- Abdel Aal G.Z., Atekwana E.A., Slater L.D., Atekwana E.A., (2004), Effects of microbial processes on electrolytic and interfacial electrical properties of unconsolidated sediments, *Geophysical Research Letters*, **31**, 1-4.
- Allen J.P., Atekwana E.A., Atekwana E.A., Duris J.W., Werkema D.D., Rossbach S., (2007), The microbial community structure in petroleum-contaminated sediments corresponds to geophysical signatures, *Applied and Environmental Microbiology*, **73**, 2860-2870.
- Asiabadi F.I., Mirbagheri S.A., Najafi P., Moatar F., (2018), Concentrations of petroleum hydrocarbons at different depths of soil following phytoremediation,

- Environmental Engineering and Management Journal*, **17**, 2129-2135.
- Atekwana E.A., Sauck W.A., Werkema Jr D.D., (2000), Investigations of geoelectrical signatures at a hydrocarbon contaminated site, *Journal of Applied Geophysics*, **44**, 167-180.
- Atekwana E.A., Sauck W.A., Abdel Aal G.Z., Werkema Jr D.D., (2002), Geophysical investigation of vadose zone conductivity anomalies at a hydrocarbon contaminated site: implications for the assessment of intrinsic bioremediation, *Journal of Environmental and Engineering Geophysics*, **7**, 103-110.
- Atekwana E.A., Werkema Jr D.D., Duris J.W., Rossbach S., Atekwana E.A., Sauck W.A., Cassidy D.P., Means J., Legall F.D., (2004a), In-situ apparent conductivity measurements and microbial population distribution at a hydrocarbon-contaminated site, *Geophysics*, **69**, 56-63.
- Atekwana E.A., Atekwana E.A., Rowe R.S., Werkema Jr D.D., Legall F.D., (2004b), The relationship of total dissolved solids measurements to bulk electrical conductivity in an aquifer contaminated with hydrocarbon, *Journal of Applied Geophysics*, **56**, 281-294.
- Atekwana E.A., Atekwana E., Legall F.D., Krishnamurthy R.V., (2004c), Field evidence for geophysical detection of subsurface zones of enhanced microbial activity, *Geophysical Research Letters*, **31**, 1-5.
- Atekwana E.A., Atekwana E.A., Werkema D.D., Allen J.P., Smart L.A., Duris J.W., Cassidy D.P., Sauck W.A., Rossbach S., (2004d), Evidence for microbial enhanced electrical conductivity in hydrocarbon-contaminated sediments, *Geophysical Research Letters*, **31**, 1-4.
- Atekwana E.A., Atekwana E.A., (2010), Geophysical signatures of microbial activity at hydrocarbon contaminated sites: A review, *Surveys in Geophysics*, **31**, 247-283.
- Atekwana E.A., Mewafy F.M., Abdel Aal G., Werkema D.D., Revil A., Slater L.D., (2014), High-resolution magnetic susceptibility measurements for investigating magnetic mineral formation during microbial mediated iron reduction, *Journal of Geophysical Research: Biogeosciences*, **119**, 80-94.
- Atlas R.M., (1975), Effects of temperature and crude oil composition on petroleum biodegradation, *Applied Microbiology*, **30**, 396-403.
- Bekins B.A., Godsy E.M., Warren E., (1999), Distribution of microbial physiologic types in an aquifer contaminated by crude oil, *Microbial Ecology*, **37**, 263-275.
- Benson A.K., Payne K.L., Stubben M.A., (1997), Mapping groundwater contamination using DC resistivity and VLF geophysical methods—a case study, *Geophysics*, **62**, 80-86.
- Bobra M., (1992), Solubility behaviour of petroleum oils in water, Environment Canada, On line at: <https://www.bsee.gov/sites/bsee.gov/files/osrr-oil-spill-response-research/120ax.pdf>.
- Bossert I.D., Kosson D.S., Hurst C.J., Knudsen G.R., McInerney M.J., Stetzenbach L.D., Walter M.V., (1997), Methods for measuring hydrocarbon biodegradation in soils, *Manual of Environmental Microbiology*, 738-745.
- Brusseau M.L., (1998), The impact of physical, chemical and biological factors on biodegradation, *Proceedings of the International Conference on Biotechnology for Soil Remediation: Scientific Bases and Practical Applications*, **1998**, 81-98.
- Caterina D., Orozco A.F., Nguyen F., (2017), Long-term ERT monitoring of biogeochemical changes of an aged hydrocarbon contamination, *Journal of Contaminant Hydrology*, **201**, 19-29.
- Ch S.R., Chandrashekar V., (2014), Detecting oil contamination by Ground Penetrating Radar around an oil storage facility in Dhanbad, Jharkhand, India, *Journal of Indian, Geophysical Union*, **18**, 448-454.
- Chaillan F., Le Flèche A., Bury E., Phantavong Y.H., Grimont P., Saliot A., Oudot J., (2004), Identification and biodegradation potential of tropical aerobic hydrocarbon-degrading microorganisms, *Research in Microbiology*, **155**, 587-595.
- Chambers J.E., Wilkinson P.B., Wealthall G.P., Loke M.H., Darden R., Wilson R., Allen D., Ogilvy R.D., (2010), Hydrogeophysical imaging of deposit heterogeneity and groundwater chemistry changes during DNAPL source zone bioremediation, *Journal of Contaminant Hydrology*, **118**, 43-61.
- Comfort S., Zlotnik V., Halihan T., (2009), Using electrical resistivity imaging to evaluate permanganate performance during an in situ treatment of a RDX-contaminated aquifer, ESTCP Project ER-0635, On line at: <https://clu-in.org/download/techfocus/chemox/ER-0635-FR-1.pdf>.
- Cooney J.J., (1984), *The Fate of Petroleum Pollutants in Fresh Water Ecosystems*, In: *Petroleum Microbiology*, Atlas R.M., (Ed.), Macmillan, New York, 399-434.
- Cooney J.J., Silver S.A., Beck E.A., (1985), Factors influencing hydrocarbon degradation in three freshwater lakes, *Microbial Ecology*, **11**, 127-137.
- Cozzarelli I.M., Baedecker M.J., Eganhouse R.P., Goerlitz D.F., (1994), The geochemical evolution of low-molecular-weight organic acids derived from the degradation of petroleum contaminants in groundwater, *Geochimica et Cosmochimica Acta*, **58**, 863-877.
- Cozzarelli I.M., Bekins B.A., Baedecker M.J., Aiken G.R., Eganhouse R.P., Tuccillo M.E., (2001), Progression of natural attenuation processes at a crude-oil spill site: I. Geochemical evolution of the plume, *Journal of Contaminant Hydrology*, **53**, 369-385.
- Cozzarelli I.M., Eganhouse R.P., Baedecker M.J., (1990), Transformation of monoaromatic hydrocarbons to organic acids in anoxic groundwater environments, *Environmental Geology and Water Science*, **16**, 135-141.
- Dahlin T., Johansson S., (1995), *Resistivity Variations in an Earth Embankment Dam in Sweden*, The 1st Meeting Environmental and Engineering Geophysics, September, 25-27, Torino, Italy.
- Daniels J.J., Roberts R., Vendl M., (1995), Ground penetrating radar for the detection of liquid contaminants, *Journal of Applied Geophysics*, **33**, 195-207.
- Das N., Chandran P., (2011), Microbial degradation of petroleum hydrocarbon contaminants: an overview, *Biotechnology Research International*, **2011**, 1-13.
- Delille D., Coulon, F., Pelletier E., (2004), Effects of temperature warming during a bioremediation study of natural and nutrient-amended hydrocarbon-contaminated sub-Antarctic soils, *Cold Regions Science and Technology*, **40**, 61-70.
- DeRyck S.M., Redman J.D., Annan A.P., (1993), *Geophysical Monitoring of a Controlled Kerosene Spill*, Symp. on the Application of Geophysics to Engineering and Environmental Problems, SAGEEP '93, San Diego, CA, 5-19.

- Dibble J.T., Bartha R., (1979), Effect of environmental parameters on the biodegradation of oil sludge, *Applied and Environmental Microbiology*, **37**, 729-739.
- Domenico P.A., Schwartz F.W., (1998), LNAPLs and DNAPLs, *Physical and Chemical Hydrogeology*, **506**, 398-411.
- Gebrekristos R.A., Pretorius J.A., Usher B.H., (2008), Determining the presence of DNAPL from field observations, In: *Manual for Site Assessment at DNAPL Contaminated Sites in South Africa*, Water Research Commission, 7-32.
- Haack S.K., Bekins B.A., (2000), Microbial populations in contaminant plumes, *Hydrogeology Journal*, **8**, 63-76.
- Hiebert F.K., Bennett P.C., (1992), Microbial control of silicate weathering in organic-rich ground water, *Science*, **258**, 278-281.
- Johansson S., Dahlin T., (1996), Seepage monitoring in an earth embankment dam by repeated resistivity measurements, *European Journal of Engineering and Environmental Geophysics*, **1**, 229-247.
- Karaoulis M.C., Kim J.H., Tsourlos P.I., (2011), 4D active time constrained resistivity inversion, *Journal of Applied Geophysics*, **73**, 25-34.
- Lien B.K., Enfield C.G., (1998), Delineation of subsurface hydrocarbon contaminant distribution using a direct push resistivity method, *Journal of Environmental & Engineering Geophysics*, **2**, 173-179.
- Loke M.H., Barker R.D., (1996), Rapid least-squares inversion of apparent resistivity pseudosections by a quasi-Newton method 1, *Geophysical Prospecting*, **44**, 131-152.
- Loke M.H., (1999), Electrical imaging surveys for environmental and engineering studies, A practical guide to 2D and 3D surveys, 8-28, On line at: https://pdfs.semanticscholar.org/efa9/43ffb44f5a217e2d22255f7e334778932248.pdf?_ga=2.156224569.344805245.1577901064-1599913487.1556049226.
- Loke M.H., (2009), Res2Dinv and Res3dinv Software Version 3.59, Geoelectrical Imaging 2D&3D, Penang, Malaysia.
- Mazác O., Benes L., Landa I., Maskova A., (1990), Determination of the extent of oil contamination in groundwater by geoelectrical methods, *Geotechnical and Environmental Geophysics*, **2**, 107-216.
- Mazac O., Kelly W.E., Landa I., (1987), Surface geoelectrics for groundwater pollution and protection studies, *Journal of Hydrology*, **93**, 277-294.
- NRC, (1993), National Research Council, In situ bioremediation: When does it work?, National Academies Press, Washington, DC, On line at: <https://doi.org/10.17226/2131>.
- Noel C., Gourry J.C., Deparis J., Blessing M., Ignatiadis I., Guimbaud C., (2016), Combining geoelectrical measurements and CO₂ analyses to monitor the enhanced bioremediation of hydrocarbon-contaminated soils: a field implementation, *Applied and Environmental Soil Science*, Article ID 1480976, doi: doi.org/10.1155/2016/1480976.
- Orozco A.F., (2012), Characterization of contaminated sites and monitoring of processes accompanying bioremediation using spectral induced polarization imaging, On line at: <http://hss.ulb.uni-bonn.de/2012/2988/2988.pdf>.
- Panthulu T.V., Krishnaiah C., Shirke J.M., (2001), Detection of seepage paths in earth dams using self-potential and electrical resistivity methods, *Engineering Geology*, **59**, 281-295.
- Pelletier E., Delille D., Delille B., (2004), Crude oil bioremediation in sub-Antarctic intertidal sediments: chemistry and toxicity of oiled residues, *Marine Environmental Research*, **57**, 311-327.
- Sauck W.A., Atekwana E.A., Nash M.S., (1998), High conductivities associated with an LNAPL plume imaged by integrated geophysical techniques, *Journal of Environmental and Engineering Geophysics*, **2**, 203-212.
- Schwartz N., Shalem T., Furman A., (2014), The effect of organic acid on the spectral-induced polarization response of soil, *Geophysical Journal International*, **197**, 269-276.
- Seferou P., Soupios P., Candasayar E., Papadopoulos N., Sarris A., Aktarakçi H., (2012), *Monitoring of Contaminant Transport by Using Geoelectrical Resistivity Tomography*, CRETE 2012 3rd Int. Conf. on Industrial and Hazardous Waste Management, Chania/Greece, **2012**, 2-7.
- Shevnin V., Mousatov A., Nakamura-Labastida E., Delgado-Rodríguez O., Mejía-Aguilar A., Sánchez-Osio J.L., Sánchez-Osio, H., (2003, April), *Study of Oil Pollution in Airports with Resistivity Sounding*, 16th EEGS Symposium on the Application of Geophysics to Engineering and Environmental Problems, 1-10.
- Song S.H., Song Y., Kwon B.D., (2005), Application of hydrogeological and geophysical methods to delineate leakage pathways in an earth fill dam, *Exploration Geophysics*, **36**, 92-96.
- Tait N.G., Davison R.M., Whittaker J.J., Leharne S.A., Lerner D.N., (2004), Borehole optimisation system (BOS)-a GIS based risk analysis tool for optimising the use of urban groundwater, *Environmental Modelling and Software*, **19**, 1111-1124.
- Thavasi R., Jayalakshmi S., Balasubramanian T., Banat I.M., (2007), Effect of salinity, temperature, pH and crude oil concentration on biodegradation of crude oil by *Pseudomonas aeruginosa*, *Journal of Biological and Environmental Sciences*, **1**, 51-57.
- Tsourlos P., Ogilvy R., Meldrum P., Williams G., (2003), Time-lapse monitoring in single boreholes using electrical resistivity tomography, *Journal of Environmental and Engineering Geophysics*, **8**, 1-14.
- Urish D.W., (1983), The Practical Application of Surface Geoelectrics to Detection of Ground-water Pollution, *Ground Water*, **21**, 144-152.
- Venosa A.D., Zhu X., (2003), Biodegradation of crude oil contaminating marine shorelines and freshwater wetlands, *Spill Science and Technology Bulletin*, **8**, 163-178.
- Von Lau E., Gan S., Ng H., (2018), Multiple stage cross-current extraction using vegetable oil in the remediation of polycyclic aromatic hydrocarbons-contaminated soil, *Environmental Engineering and Management Journal*, **17**, 63-70.
- Werkema D.D., Atekwana E.A., Endres A.L., Sauck W.A., Cassidy D.P., (2003), Investigating the geoelectrical response of hydrocarbon contamination undergoing biodegradation, *Geophysical Research Letters*, **30**, 1647.
- Yang C.H., Yu C.Y., Su S.W., (2007), High resistivities associated with a newly formed LNAPL plume imaged by geoelectric techniques-a case study, *Journal of the Chinese Institute of Engineers*, **30**, 53-62.